Diffusion in a Variable Aperture Slot: Impact on Radionuclide Release from a Repository for Spent Fuel

Helen Winberg-Wang

⊗ANS

Check for updates

Diffusion in a Variable Aperture Slot: Impact on Radionuclide Release from a Repository for Spent Fuel

Helen Winberg-Wang ⃝*

Royal Institute of Technology, Department of Chemical Engineering, Stockholm, Sweden

Abstract — *Diffusion experiments under stagnant conditions in a constant aperture and a variable aperture slot were made to obtain data for simulation of simultaneous flow and diffusion in fractures. This approach was necessitated by the need to avoid buoyancy-induced flow caused by density differences generated by the presence of a tracer. For this purpose, to avoid flow but negligibly influence diffusion the slots were filled with agar, which generates a 99% porous matrix, which negligibly affects diffusion but essentially stops flow. A simple photographic technique was used to follow diffusion and to determine the aperture distribution on the variable aperture slot. With the obtained data, numerical simulations were performed to illustrate how a solute diffuses from a source into the water seeping past. The results support the simple analytical solution that has been used to determine the escape of radionuclides from a damaged canister containing spent nuclear fuel in a geologic repository in fractured rock.*

Keywords — *Solute diffusion, rock fracture diffusion, radionuclide escape.*

Note — *Some figures may be in color only in the electronic version.*

I. INTRODUCTION AND BACKGROUND

Analysis of fluid flow and solute transport in fractured rock is an integral aspect of assessing the suitability of a geologic repository for long-term storage of radioactive nuclear waste. To quantify the potential release of radionuclides to the surrounding environment the concept of an equivalent flow rate Q_{eq} has been suggested by Neretnieks.[1] It is used to define in an illustrative way the rate of mass transfer between a deposition hole with nuclear waste and the water that seeps in fractures that intersect the hole. The mass transfer rate N of molecular size solutes with concentration c_o at the clay-water interface is given by

$$N = Q_{eq} \cdot c_o \ , \tag{1}$$

where $c_o = c_i - c_w$, with c_i the concentration at the buffer-water interface and c_w the concentration in the incoming water. A simple analytical expression for Q_{eq} is available for constant aperture fractures. This will be shown and discussed later. The concept has been used in SKB's safety analyses since 1979 (KBS-3) and also recently in the latest Swedish (SKB, Ref. 2) and Finnish (Posiva Report[3]) performance assessments submitted to the authorities to obtain permits to build the repositories. The simple model has been verified by numerically "exact" solutions of the underlying flow and diffusion equation.[4] Simulations by Liu and Neretnieks[5,6] have shown that the concept and the model give fair approximations for variable aperture fractures.

Because of its central role in release modeling and its seeming simplicity it has been suggested that the concept of equivalent flow rate should be better supported by, if possible, illustrative experiments that readily can be grasped by persons less familiar with diffusion and its modeling.

Direct experimental illustration of the mass transfer has been made by letting dyes diffuse into narrow slots

with stagnant and seeping water. The slots were constructed of two glass sheets with planar as well as undulating surfaces. The latter forms a variable aperture slot that illustrates and substitutes for a real variable aperture fracture in granite. Cast replicas of a real fracture in granite have also been made and used in experiments. In the experiments with seeping water in the slots, it was found that even minute density differences between pure water and water with dye severely influenced and changed the imposed velocity profiles and even induced circulation patterns. This prohibited the use of this technique because the disturbances could not be controlled. Even normal lighting in the laboratory could heat water with dye causing the dyed water to heat up slightly and start circulation.

In this paper, another technique is used, which avoids the problem with buoyancy effects; this technique uses an agar-gel to suppress flow. However, this approach needs a proof that continuous flow through the fracture can be replaced by intermittent exchange of water in the fracture with the same mean flow rate as that caused by flow. This is also presented in this paper.

This paper aims to illustrate the rate of mass transfer described by the Q_{eq} model also for variable aperture fractures by experiments and simulations. Experiments are used to study the migration of solutes by diffusion in variable aperture slots, which have more rock-like properties compared to parallel slots. The diffusion coupled with flow in the variable aperture slot is simulated using COMSOL® Multiphysics.

This paper does not investigate the effect of density gradients but focuses on constant density systems. Density gradients are unarguably of great importance when modeling diffusion and flow at sites for final repositories. Density gradients can arise both due to temperature gradients and differences in salinities in the incoming water. However, this is outside the scope of the present paper and will be treated in another paper.

II. CONCEPTUALIZATION AND ANALYTICAL EXPRESSION

Our analysis considers a deposition hole for high-level waste intersected nearly perpendicularly by a fracture, see Fig. 1.

Figure 2a illustrates the flow field in the fracture. The water flows around the impervious backfill surrounding the waste canister. This results in a cylindrical contact area. At the clay-water interface the concentration of solute is c_i. The incoming water flows from left to right, with a concentration c_w. When passing the interface, the water picks up the diffusing solute.
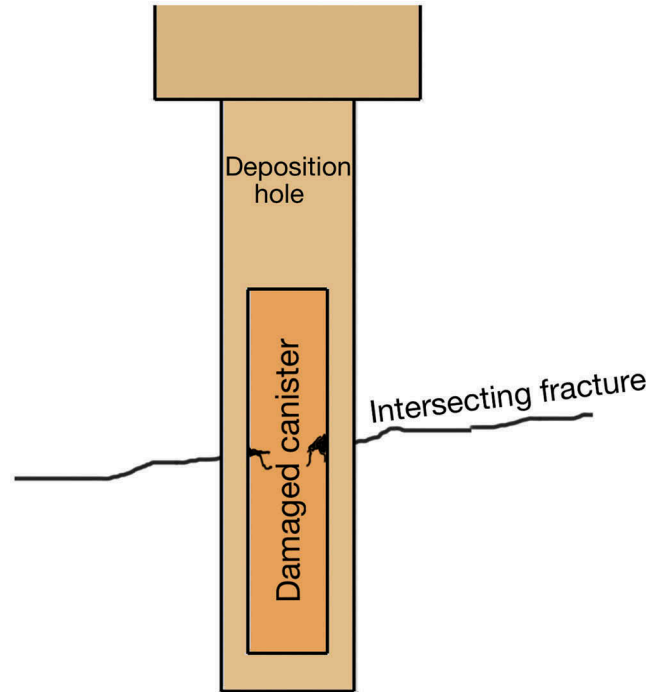

Fig. 1. Illustration of fracture intersecting a deposit hole with a damaged leaking copper canister.

The solute diffuses farther and farther out into the water seeping past, which gathers more and more solute the farther along the interface it flows. By the time the water leaves the interface it has picked up a certain amount of solute. The amount of the solute that leaves with the water depends on the contact time between the water and the interface, the interface area, and the rate of diffusion of the solute.

When the concentration boundary layer is thin in comparison with the radius of the deposition hole it can be "unwound" and straightened as shown in Fig. 2b, which shows one side to the object. In a coordinate system with x (m) in the flow direction and y (m) in the cross-stream direction, the concentration $c(y)$ as it evolves over time t (which is proportional to how far along the object the water has traveled) can be described by the solution to the diffusion equation for the situation where there is diffusion upward in the y direction.[7] Diffusion in the flow direction is assumed to be negligible, which is a good approximation when the penetration depth of the front is short in comparison to the travel distance:

$$c(t,y) = c_o erfc\left(\frac{y}{2\sqrt{D_w\,t}}\right) \ . \quad (2)$$

The mean penetration depth at location x can be determined by
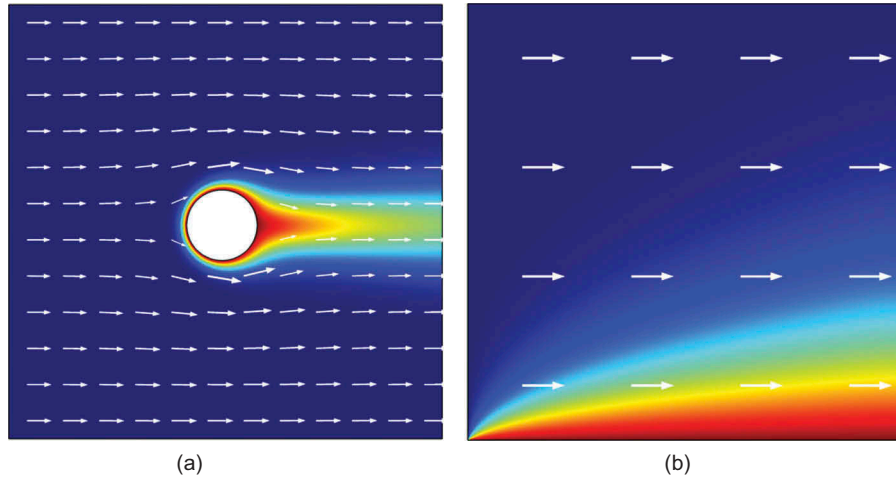
(a)   (b)

Fig. 2. Illustration of water seeping in a fracture intersecting a deposition hole and solute diffusing into the water around (a) a cylindrical deposit hole and (b) a linearized case where the interface has been unwound and straightened.

$$\eta_{mean}(t) = \frac{1}{c_o} \int_0^\infty c(t,y)dy = \frac{2}{\sqrt{\pi}} \sqrt{D_w t} \ . \qquad (3)$$

The mass transfer rate N is given by

$$N(t) = c_o u \ b \ \eta_{mean}(t) = c_o \frac{2}{\sqrt{\pi}} b \ u \sqrt{D_w t} \ , \qquad (4)$$

where

u = approaching water velocity (m/s)

b = slot aperture (m)

D_w = diffusion coefficient (m^2/s)

t = time since the diffusion started (s).

Equation (4) is valid for the straight flow path. For flow around the cylinder on one side, the same equation is valid,[8] but the constant $\frac{2}{\sqrt{\pi}}$ in Eq. (4) is then 13% larger. It may be noted that in the linear case the velocity is constant in the slot because in the narrow slot friction against the walls dominates the flow resistance. Therefore, the friction against the bottom of the slot can be neglected when η_{mean} is larger than the slot aperture.

When this condition is fulfilled and when the diffusion in the flow direction is negligible the concentration profile and the mass uptake into the water is the same for the case when the water is stagnant and has been exposed to the source during time t as for the case when the water has flown with the constant velocity past the source during the same time. As a result of negligible diffusion in the x direction, the time t can be substituted for $t = x_o/u$, where u is the water velocity in the

x direction. From Eq. (4) the mass N transported past position x_o is

$$N(x) = c_o 2b \sqrt{\frac{D_w x_o u}{\pi}}. \qquad (5)$$

Hence if it can be experimentally shown that the mass uptake over time evolves as Eq. (4) this implies that Eq. (5) is valid.

III. EXPERIMENTAL

For the experiments, two setups were built. The main idea is to construct an artificial fracture with a variable aperture and expose the bottom boundary to a dye source. The first setup is equipped with two sheets of flat glass to serve as a reference and the second setup is built with a slot of two sheets of wavy glass to simulate a rock fracture with variable aperture.

The slots are placed in front of a light source so that the transmitted light can be documented by the camera placed in front of the slot, see Fig. 3. The aperture field is measured by comparing the light extinction of a dye-filled fracture to the light extinction of a dye-filled calibration slot with known aperture. The aperture in the fracture is determined by using Lambert-Beer law, similar to methods common for investigating fracture flow.[9,10] The calibration slot is used to determine any nonlinearity in the camera sensitivity and in lighting intensity variations over the source. The concentration profile evolution is determined by photographing the setup at regular intervals.
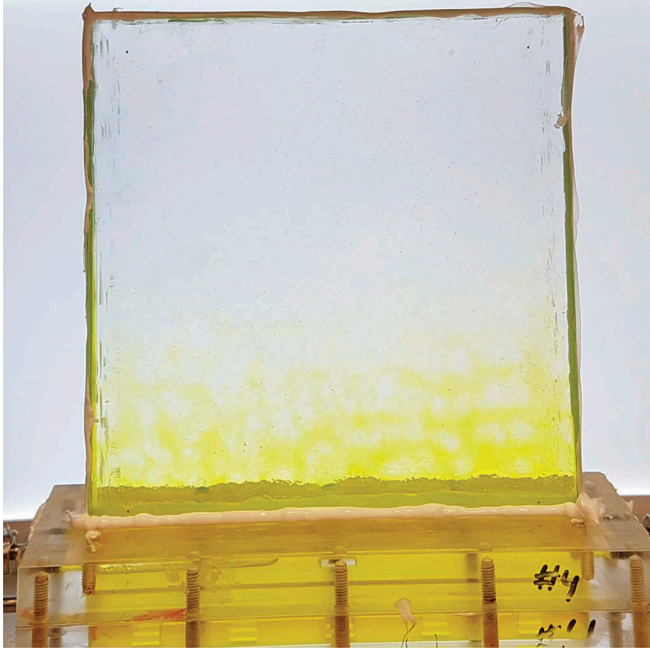
Fig. 3. Experimental setup: The variable fracture setup is placed in front of a light board.

III.A. Parallel Fracture Setup

The first setup with a parallel slot was used to determine the diffusion coefficient and to test the rigor of the method. The parallel slot was created by separating two sheets of glass (100 × 150 × 3.84 mm) with plastic spacers. The slot is kept in place by a base of Plexiglas and sealed by silicon glue on the other three sides. To avoid air intrusion through the silicon seals during the long runs the silicon sides are covered with strips of Parafilm. The Parafilm hinders diffusion of air and water vapor through the silicon in and out of the setup. To prevent convection due to local density differences the slot was filled with an agar medium. Diffusion of Uranine in agar is well documented and at agar concentrations of 0.5% to 2% there is negligible effect on the diffusion rate.[11–14] The agar medium acts like a very sparse network of very large intertwined molecules within which water and dye can diffuse freely but in which water is hindered to flow due to the low hydraulic conductivity of the agar. The base of the slot is connected to a dye reservoir.

The agar medium is prepared by mixing 2.5 g of agar powder into 250 ml of deionized water; the solution is thereafter boiled until it becomes a clear liquid. This warm liquid is poured on top of a warm glass sheet surrounded by a frame. Another piece of warm glass is slowly tilted onto the agar sandwiching a thin agar layer in between. For the parallel plate slot spacers were used

to assure a constant thickness of the agar layer. Afterward, the agar is left to cool and harden. After the agar has hardened, three of the slot sides are sealed with silicon and strips of Parafilm. Next, the slot is submerged in a water bath for the silicon to harden without risking the agar to dry.

To measure the concentration in the parallel slot and fracture, Lambert-Beer law (see Sec. III.E) is used in combination with the light absorption of the dye. A light board is placed behind the setup to provide background lighting and a camera (Nikon D90) is placed in front of the setup to measure the light transmitted through the setup. The setup is placed in a dark box between photoshoots. The dark box reduces dye degradation due to prolonged light exposure. Tests have found the degradation to be negligible in this setup. The camera is connected to a computer for taking a photo each day (Camera Control Pro 2, commercially available software from Nikon). The room is kept dark during the test.

III.B. Variable Aperture Setup

The second setup with a variable aperture is built in the same way as the parallel slot setup. However, instead of plain glass, the variable aperture fracture is created by closely aligning two pieces (150 × 150 mm) of shower cabin glass to provide a system with a variable aperture. The variable aperture setup has a larger dye reservoir of ~37 ml. It may be noted that earlier manufacture of variable aperture slots by casting transparent epoxy from real granite fracture faces as described in Refs. 10 and 15 was found to be unsuitable for long-time experiments. After prolonged exposure, the surfaces became tainted due to dye diffusion into the porous epoxy medium, so that the camera records not only dye in the water in the slot but also on and in the epoxy.

A calibration slot is present adjacent to the variable aperture slot. The calibration slot is used to determine both the aperture and the concentration of dye in the variable aperture fracture. The calibration slot is constructed of two plain glass plates with the same dimensions as the glass plates used for the parallel slot. The calibration slot is in the form of a wedge. The aperture ranges from 0 mm at the bottom to 1.49 mm at the top. The bottom and sides are sealed with silicon and the outside is equipped with a ruler starting from the bottom, as a tool for reference. For calibration purposes, the slot is filled with a fraction of the dye chamber concentration c_o.

⊗ANS

With the aperture and the concentration of the dye c_o of the calibration slot known the variable aperture slot after being emptied of the agar is filled with the same dye solution with the same concentration. To avoid disturbing the alignment of the glass sheets the aperture distribution of the slot cannot be determined beforehand. It is determined after the diffusion phase by driving out the agar and filling it with a dye solution. Thereby, the aperture in the variable aperture slot can be determined by comparing the intensity in each point with the intensity in the calibration slot, after adjusting for any unevenness in the background lighting. The unevenness is determined by photographing the light source and accurately locating the fix points that were used to identify the location of the light source. The resolution of the camera was about 3 to 4 million pixels, which gives a spatial resolution of less than 0.1 mm.

III.C. Uranine

Uranine was used for the described experiments. It is a dye commonly used in tracer experiments. Uranine was chosen because of its high color intensity even at low concentrations and its relatively small molecule size, 332.30 g/mol (Ref. 16). According to Ref. 14, the diffusion coefficient for Uranine in water at 20°C is $4.88 \cdot 10^{-10} \, \text{m}^2/\text{s}$.

To avoid light degradation the experimental setups are kept in darkness between photoshoots. The dye degrades insignificantly during 4 weeks. The light degradation in a calibration slot was also monitored by weekly extracting samples. The samples were then measured with an UV-Vis spectrophotometer at 494 nm (Thermo Scientific Genesys 10S).

III.D. Experiments

A dye solution was injected into the dye chamber at the bottom of the slot at the start of the experiment. The solution was made by dissolving 0.042 g Uranine in 250 ml degassed deionized water for the parallel slot and 0.093 g Uranine in 100 ml water for the variable aperture slot. Next, the setup was sealed and a photograph was taken manually about once a day for 3 weeks until aborted due to air intrusions.

III.E. Picture Evaluation

In order to determine the dye diffusion rate into the slots, it is necessary to determine the aperture of the slots and the concentration in the fracture at given points in time from the experimental images. The images have been processed with Matlab®. The underlying methodology is described below.

For the parallel slot, the aperture is known but to determine variable slot aperture and the concentration of solute in the slots at any given time, Lambert-Beer law is used. This relation describes the intensity of the transmitted light I_s as a function of the local aperture h and solute concentration c. ϵ is the extinction coefficient for the dye. It is determined for the wavelength used from the calibration slot:

$$\frac{I_s}{I_0} = e^{-\epsilon c h} \, , \tag{6}$$

where I_0 is the intensity of the incoming light.

Equation (6) is used as follows. The photographs record data for three colors: red, green, and blue. Uranine concentration in the concentration range used is best evaluated by measuring the blue transmissivity. First, the photos are intensity calibrated by dividing the intensity I_s of each pixel with the background intensity I_0 in that location to determine any unevenness of the incoming light I_0. This slight unevenness, totaling a few percent, was compensated for when using Eq. (6) to evaluate the aperture distribution and the concentration evolution. The unevenness correction also accounts for the gradual light fall-off at the off-center locations of the camera sensor. The change in background lighting with time is also corrected for. This seldom exceeds 3% over the month-long experiment.

The aperture distribution is determined by utilizing a calibration slot, which is present beside the diffusion slot in the photographs. The known aperture and concentration in the calibration slot is used to determine the light extinction coefficient ϵ. With this, the aperture in the fractures is determined from the known constant concentration. The aperture of the visual part of the variable aperture slot is reduced to a 124×124 matrix, $1 \, \text{mm}^2$/voxel, to save computational time for the COMSOL Multiphysics simulations. The fine structures lost by lumping pixels into 1×1 mm are acceptable because in the slot any differences are evened out by diffusion during a time of about 1 h by diffusion.

To account for the areas not available for the camera, 16 mm high (Fig. 4), the aperture in the hidden area is taken as the mean in the x direction and further extrapolated in the negative y direction using the trend of the decreasing aperture toward the lower end.

IV. MATHEMATICAL MODEL FOR MIGRATION IN SEEPING WATER

A numerical routine was developed to simulate the experiments. In the simulations, a two-dimensional (2-D)
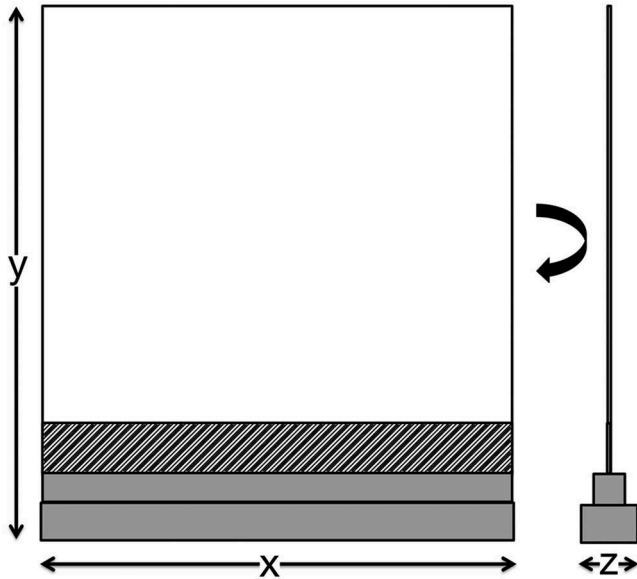
Fig. 4. Setup illustration: White shows the visible part of the variable aperture slot, gray-solid indicates the dye chamber, and dashed area shows the hidden region 16 mm high.

computational domain is considered. The simulation provides a concentration field in two dimensions. With this information, it is then also possible to simulate a flow field and concentration field in two dimensions as if flow were imposed.

For the computational domain, the slot shown in Fig. 4 is considered. In physical space, it consists of a slot between near parallel plates, with varying aperture. The aperture is denoted by $b = b(x, y)$. The flow is in the positive x direction and is laminar. Details in the z direction are omitted with the argument that the concentration across the aperture is rapidly evened out by diffusion. The characteristic time for this is

$$t_c = \frac{\left(\frac{d}{2}\right)^2}{D_w} = \frac{10^{-6}}{10^{-9}} = 1000 \text{ s}$$

for a $d = 2$ mm aperture fracture.[7] This is very much shorter than the times of interest in this experiment.

The aperture field is used to determine the flow field $u = u(x, y)$ for a given pressure head difference over the slot. The simulation of the flow in the fracture is done by applying the cubic law of the aperture, which states that the local hydraulic conductivity is proportional to the aperture to the third power.[17] For the flow simulation, the flowrate Q is taken to be the residence times of 7 days for the parallel slot and 21 days the variable aperture slot.

From this, a mean hydraulic head difference is determined by solving the Darcy flow for the variable aperture fracture. The Darcy flow can be described by Eq. (7):

$$\boldsymbol{Q} = A\boldsymbol{u} = -k\frac{A\rho g}{\mu}\nabla H \ , \tag{7}$$

where

∇H = hydraulic gradient

A = cross-sectional area for flow

g = gravitational constant

ρ = density

μ = viscosity of water,

and where the permeability k is assumed to be equal to that for flow in a slot with smooth parallel walls in each point, $k = b^2/12$. This gives hydraulic gradients of $9.7 \cdot 10^{-12}$ and $1.8 \cdot 10^{-10}$ m/m for the constant and the variable aperture slot, respectively.

This illustrates the difficulty to make experiments with imposed flow because relative density differences of the same magnitudes caused by local concentration differences will cause gravity-induced flow in horizontal as well as sloping and vertical fractures. This problem is avoided by the presence of the agar which stops flow.

To describe the water flow and solute transport in a fracture with variable aperture, the model needs to consider both the variable flow field and the effect on the diffusion caused by the variation in aperture. In the system of interest, the water is seeping and is regarded to be laminar and incompressible. For steady-state flow, the law of conservation of mass gives $\nabla \cdot \boldsymbol{Q} = 0$, leading to the Reynolds' equation[17]:

$$\nabla \cdot \boldsymbol{Q} = \nabla \cdot \left(-\frac{\rho g}{12\mu}b^3\nabla H\right) = 0 \ . \tag{8}$$

The Reynolds's equation [Eq. (8)] can be used to describe the flow of water in fractures in rock, and in this study, the potential flow and diffusion is computed using COMSOL Multiphysics (Ref. 18). Table I summarizes the data used in the steady-state simulations.

Once the flow field $\boldsymbol{u}$ has been determined by the solution of Eq. (8), the time-dependent diffusion-convection is used to describe how the concentration distribution changes with time and in space. The three-dimensional diffusion-convection equation is reduced to a 2-D equation. In a thin fracture, it can be modeled as a 2-D fracture because

⊗ANS

TABLE I

Steady-State Simulation

Parameter	Value	Description
L_{con}	0.1 (m)	Slot length constant aperture slot
L_{var}	0.123 (m)	Slot length variable aperture slot
H_{slot}	0.140 (m)	Slot height
b	$b(x,y)$ (m)	Experimental aperture field
V_{ch_con}	12.5 (ml)	Volume dye chamber constant aperture slot
∇H_{con}	$9.7 \cdot 10^{-12}$ (m/m)	Hydraulic gradient
∇H_{var}	$1.8 \cdot 10^{-10}$ (m/m)	Hydraulic gradient

diffusion across the aperture evens out any differences caused by the semiparabolic velocity profile. The effective diffusivity in the flow direction is only somewhat larger than the molecular diffusion coefficient caused by Taylor dispersion. This effect is neglected also because Taylor dispersion does not have time to develop in the "rapidly" changing apertures. Then the diffusion-convection equation for a variable aperture fracture becomes

$$b\frac{\partial c_A}{\partial t} = -b\boldsymbol{u} \cdot \nabla c_A + D_w\nabla \cdot (b\nabla c_A) \ . \quad (9)$$

By expanding the right side terms of Eq. (9) and dividing by the aperture Eq. (9) becomes[5]

$$\frac{\partial c_A}{\partial t} = -u \cdot \nabla c_A + D_w\nabla^2 c_A + \frac{D_w\nabla b \cdot \nabla c_A}{b} \ . \quad (10)$$

The last term accounts for the local change in aperture in the fracture. Table II summarizes the data used for the time-dependent simulations.

At $t = 0$, the fracture is filled with only water and all dye is confined to the dye chamber. The dye diffuses into the fracture from the solute source boundary with concentration c_i. The volumes of the dye chamber for the constant and variable aperture slot are 12.5 and 37 ml, respectively, and the slot volumes are 19 and 4 ml. The concentration in the parallel slot chamber changes with time due to the relatively large aperture slot. However, exploratory calculations found that c_o is essentially constant due to the large volume relative to the fracture volume for the variable aperture slot so its variation is neglected. The top border was kept open to diffusion to simulate an infinite fracture but closed to flow.

In the simulation this assumption was found to be acceptable. The diffusion coefficient was taken to be $3.54 \cdot 10^{-10}$ m^2/s, which is the value obtained by the parallel slot test. At the outlet, $x = x_o$, the mass transfer rate is calculated by integrating the mass flux times over the whole height

$$N = \int c(y) \cdot b(y) \cdot u(y)dy \ .$$

TABLE II

Time-Dependent Simulation

Parameter	Value	Description
L_{con}	0.1 (m)	Slot length constant aperture slot
L_{var}	0.123 (m)	Slot length variable aperture slot
H_{slot}	0.14 (m)	Slot height
b	$b(x,y)$ (m)	Experimental aperture field
c_i	$c_i (x,t)$ (mol/m^3)	Concentration at bottom
c_w	0 (g/m^3)	Concentration in slot initially
D_e	$3.54 \cdot 10^{-10}$ (m^2/s)	Molecular diffusion coefficient
u	$u(x,y)$ (m/s)	Flow from the steady-state solution
V_{ch_var}	37 (ml)	Volume dye chamber variable aperture slot

This gives information on the rate of mass transfer to the water that has passed the fracture where it has been in contact with the dye source. When the outlet concentration becomes constant steady state has been reached. From this information the transfer rate and thus a value of the Q_{eq} can be obtained.

V. EXPERIMENTAL AND SIMULATION RESULTS

V.A. Experimental Results

Figure 5 shows the diffusion profiles in the visible parts of the constant aperture slot and an initial concentration $c_o = 0.16$ g/l. In this case, the concentration at the inlet to the slot c_i decreased with time and it was necessary to account for this in the evaluation. Therefore, a numerical solution of the evolution of the concentration profiles was needed. This was done by solving the diffusion equation using the Crank-Nicholson method for a constant aperture slot accounting for the decrease in the interface concentration by

$$c_i(0,t) = c_o - \frac{b}{A} \int_0^H c(y,t)dy \ .$$

By minimizing the least-square sum between all experimental and simulated concentration profiles, the diffusion coefficient with respect to D_w, the best value was $D_w = 3.54 \cdot 10^{-10}$ m^2/s. Also, c_o was used as a fitting

parameter and it was confirmed that the fit was best for $c_o = 0.16$ g/l, which was the value of the prepared initial solution.

For illustration, Fig. 6 shows the 0.1-penetration depth in comparison to the Crank-Nicolson solution.

V.B. Experimental Results for Variable Aperture Slot

Figure 7 shows the aperture distribution in the variable aperture slot. The variable aperture slot has an average aperture of 0.23 mm. It is seen that aperture increases with height. It is narrower in the bottom because it was tightly fitted into the holder. When emptying the slot of agar by heating the setup, the Plexiglas holder in which the glass sheets were inserted shrunk slightly by the heating by about 0.5%, squeezing the glass sheets even closer at the bottom, ~0.05 mm. This squeezing is compensated for when evaluating the aperture that was present during the diffusion experiment.

By utilizing the aperture field, the concentration distribution in Fig. 8 was obtained for a residence time 21 days.

When comparing the least-square sum between the concentration data and the concentration solution of the diffusion equation in two dimensions, the diffusion coefficient can be determined. This coefficient can be compared with the results from the parallel slot. This diffusion coefficient was evaluated after 21 days where D_e was found to be $4.3 \cdot 10^{-10}$ m^2/s. This value was well between the value of Ref. 14 of $4.88 \cdot 10^{-10}$ m^2/s and the value obtained from the constant aperture slot experiment $3.54 \cdot 10^{-10}$ m^2/s.
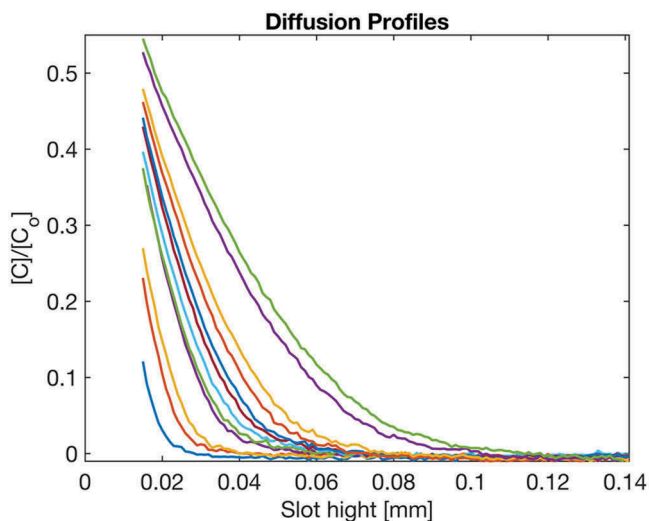

Fig. 5. Diffusion profiles for diffusion of Uranine in the visible part of the parallel slot for diffusion times of 1.1, 2.1, 3.1, 5.2, 6.1, 7.1, 8.1, 8.9, 11.2, 13.1, 23.0, and 25.9 days.
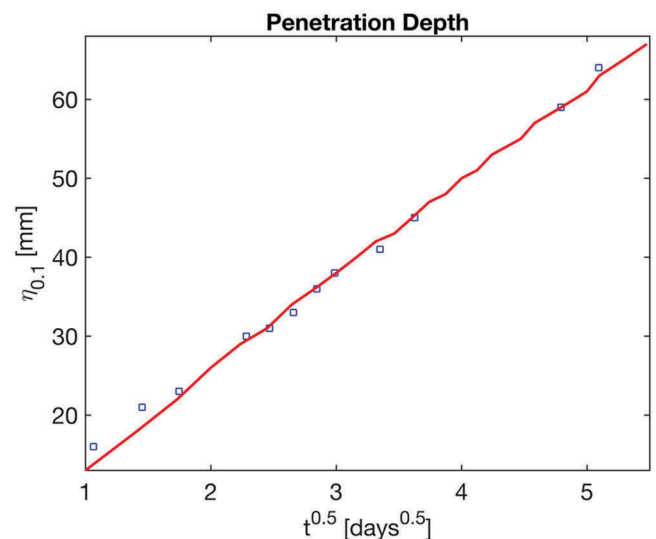

Fig. 6. Experimental and predicted penetration depth $\eta_{0.1}$ of the $c = 0.1 \cdot c_o$ front. Squares are experimental data and the solid line is Crank-Nicholson solution.
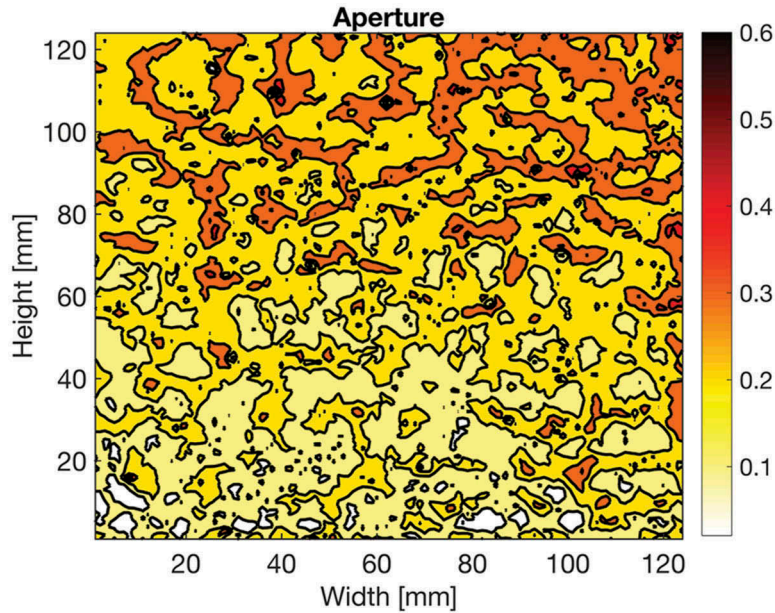
⊗ANS

Fig. 7. Aperture distribution of visible part of variable aperture fracture $< b_{vis} \geq 0.24$ mm.
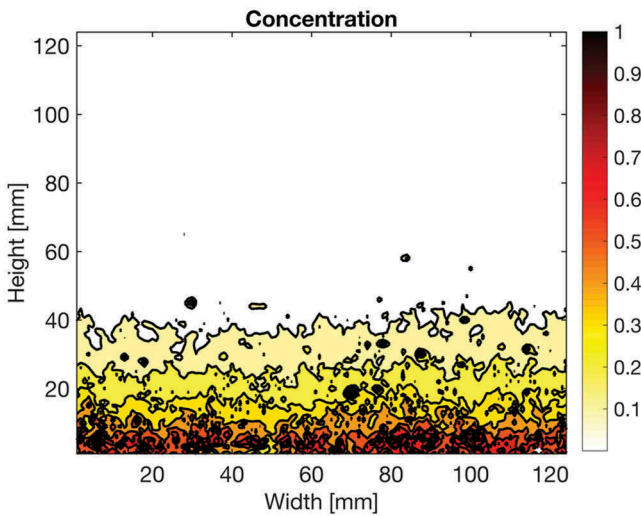

Fig. 8. Concentration in visible part of the variable slot after 21 days; 21 extreme voxels removed to enhance the figure's diffusion fronts.
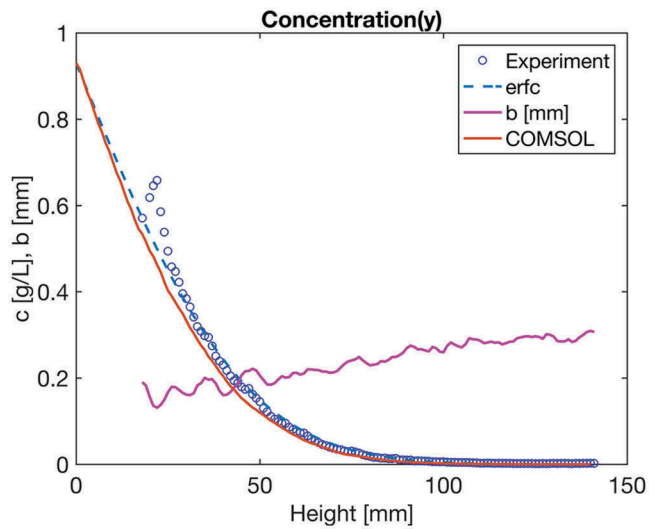

Fig. 9. Average of concentration profile in x direction in the visible part of the variable slot after 21 days. The wavy subhorizontal line is the mean aperture over the width of the slot.

Figure 9 shows the concentration profile after 21 days averaged over the entire visible part of the slot width, about 12 cm. Each circle in Fig. 9 represents a height of about 1 mm.

The experimental curve can be compared to what is predicted by the solution of the diffusion equation for the variable aperture slot, the straight curve and the dashed curve, which show the profile for a constant aperture slot with the same mean aperture as the variable aperture slot.

The peak of the left-most five points is suspected to be caused by some optical phenomenon, reflection or shading, due to the close proximity of the Plexiglas holder at the lower part of the slot.

V.C. Simulation Under Flowing Conditions

The simulations were made by applying a hydraulic gradient from left to right to obtain a flow field with residence

time of 21 days. Figure 10 shows the profile after 3 times the residence time. After three residence times have passed the concentration has stabilized and reached steady state. Integration of the concentration times the flow and aperture at the right-hand border provides $N = 1.7 \cdot 10^{-13}$ kg/s. It may be noted that the streamlines in Fig. 10 show that the flow is substantially higher in the upper part of the slot, as a form of channeling. This is seen by the smaller distance between the lines.

The same simulation procedure with constant aperture was made for the parallel slot which gave $N = 6.7 \cdot 10^{-13}$ kg/s.

By utilizing the simplified expression [Eq. (3)], with the same mean aperture as for the simulations, the mass transfer rate for the parallel and the variable aperture was determined to be $6.3 \cdot 10^{-13}$ and $4.1 \cdot 10^{-13}$ kg/s, respectively, see Table III (see also Table IV for additional results.)

VI. DISCUSSION AND CONCLUSIONS

The experimental technique in which agar is used to hinder flow induced by buoyancy forces is simple and works well. Buoyancy-induced flow is effectively hindered while only marginally influencing diffusion. The photographic method was simple and reliable. It permitted the determination of the aperture distribution of the slot. Compensation for small nonlinearities and intensities in the illuminating screen and sensitivity of the sensor in the camera could readily be made. It was found that
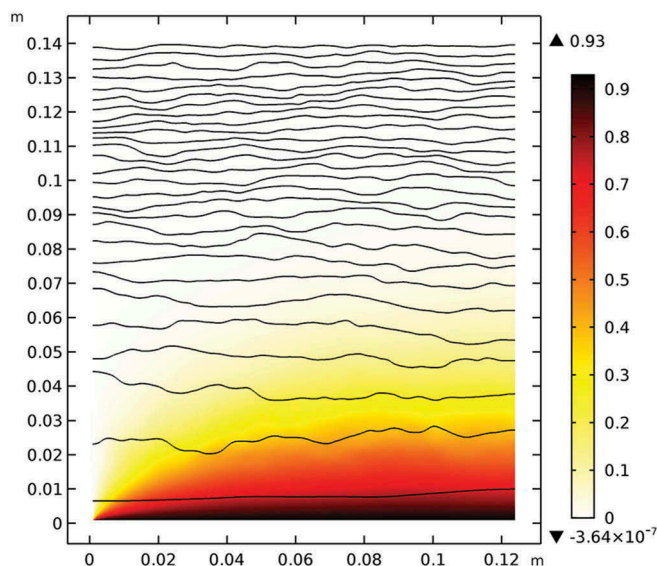

Fig. 10. Simulated concentration field after three residence times. Flow from left to right with streamlines are shown.

TABLE III

Mass Transfer Rates*

	Parallel Slot (kg/s)	Variable Slot (kg/s)
Experiment	$5.5 \cdot 10^{-13}$	$3.7 \cdot 10^{-13}$
COMSOL simulation	$6.7 \cdot 10^{-13}$	$1.7 \cdot 10^{-13}$
Simple Q_{eq} formula	$6.3 \cdot 10^{-13}$	$4.1 \cdot 10^{-13}$

*For N in kilograms per second.

TABLE IV

Additional Results

	Parallel Slot	Variable Slot
c_o (kg/m^3)	0.16	0.93
Q_{eq} experiment (m^3/yr)[a]	$4.6 \cdot 10^{-4}$	$2.5 \cdot 10^{-5}$
u (m/yr)	5.2	2.2
$<b>$ (mm)	1.46	0.23

[a]Refers to flow around a cylindrical object, e.g., 2 times the experimental value.

casting real fracture surfaces to make a good replica of these could not be later used to study flow and diffusion in the replicas because the transparent material would sorb the tracer. The numerical model agrees very well for the parallel system. However, for the variable aperture case, it also shows the effects that channeling can have on a true fracture system, which depends on the fracture shape. The experiments support the concept and equations used to assess the rate of release of radionuclides from a damaged canister in a repository for high-level waste in fractured rocks.

ORCID

Helen Winberg-Wang http://orcid.org/0000-0002-2010-2894

References

1. I. NERETNIEKS, "Transport Mechanisms and Rate of Transport of Radionuclides in the Geosphere as Related to the Swedish KBS Concept," SM-243/108, 315, International Atomic Energy Agency (1979).

2. SKB, "Radionuclide Transport Report for the Safety Assessment SR-Site," SKB Report TR-10-50 (2010); http://www.skb.com/publications/ (current as of Feb. 5, 2018).

3. "Safety Case for the Disposal of Spent Nuclear Fuel at Olkiluoto—Performance Assessment 2012, Posiva Oy (Apr. 2012); http://www.posiva.fi (current as of Feb. 5, 2018).

4. I. NERETNIEKS, L. LIU, and L. MORENO, "Mass Transfer Between Waste Canister and Water Seeping in Rock Fractures Revisiting the Q-Equivalent Model," SKB Report, TR-10-42 (2010); http://www.skb.com/publications/ (current as of Feb. 5, 2018).

5. L. LIU and I. NERETNIEKS, "Analysis of Fluid Flow and Solute Transport in a Fracture Intersecting a Canister with Variable Aperture Fractures and Arbitrary Intersection Angles," *Nucl. Technol.*, **150**, 132 (2004); https://doi.org/10.13182/NT05-A3611.

6. L. LIU and I. NERETNIEKS, "Analysis of Fluid Flow and Solute Transport in a Single Fracture with Variable Aperture Intersecting a Canister: Comparison Between Fractal and Gaussian Fractures," *Phys. Chem. Earth*, **31**, 634 (2006); https://doi.org/10.1016/j.pce.2006.04.012.

7. R. B. BIRD, W. E. STEWART, and E. N. LIGHTFOOT, *Transport Phenomena*, 2nd ed., Wiley (2007).

8. P. L. CHAMBRÉ et al., "Analytical Performance Models for Geologic Repositories," LBL-14842, Vol. 2, Lawrence Berkeley Laboratory, Berkeley, California (1982).

9. E. ISAKOV et al., "Fluid Flow Through Rough Fractures in Rocks I: High Resolution Aperture Determinations," *Earth Planetary Sci. Let.*, **191**, 267 (2001); https://doi.org/10.1016/S0012-821X(01)00424-1.

10. A. SAWADA and H. SATO, "A Study of Hydraulic Properties in a Single Fracture with In-Plane Heterogeneity: An Evaluation Using Optical Measurements of a Transparent Replica," *Nucl. Eng. Technol.*, **42**, *1*, 9 (2010); https://doi.org/10.5516/NET.2010.42.1.009.

11. D. CHAMPION et al., "Comparison Between Two Methods to Measure Translational Diffusion of a Small Molecule at Subzero Temperature," *J. Agric. Food Chem.*, **43**, *11*, 2887 (1995); https://doi.org/10.1021/jf00059a022.

12. M. MUSTAFA et al., "Dye Diffusion in Isotropic and Liquid Crystalline Aqueous (Hydroxypropyl) Cellulose," *Macromolecules*, **26**, *2*, 370 (1993); https://doi.org/10.1021/ma00054a017.

13. E. SCHANTZ and M. LAUFFER, "Diffusion Measurements in Agar Gel," *Biochemistry*, **1**, *4*, 658 (1962); https://doi.org/10.1021/bi00910a019.

14. Z. BU and P. RUSSO, "Diffusion of Dextran in Aqueous (Hydroxypropyl) Cellulose," *Macromolecules*, **27**, *5*, 1187 (1994); https://doi.org/10.1021/ma00083a017.

15. H. HAKAMI, "Water Flow in Single Rock Joints," Technical Report Stripa Project, SKB (1989); http://www.skb.com/publications/ (current as of Feb. 5, 2018).

16. R. PERRY and D. GREEN, *Perry's Chemical Engineers Handbook*, 7th ed., Table 2-2, pp. 2–38, McGraw-Hill (1997).

17. P. A. WITHERSPOON et al., "Validity of Cubic Law for Fluid Flow in Deformable Rock Fracture," *Water Resour. Res.*, **16**, 1016 (1980); https://doi.org/10.1029/WR016i006p01016.

18. COMSOL.se/model/rock-fracture-flow-101 (2012).